EUROPEAN ORGANIZATION FOR NUCLEAR RESEARCH

CERN-PPE/90-112
14th August 1990

[redacted]

BRANCHING RATIOS AND PROPERTIES OF D-MESON DECAYS

M.P. Alvarez[2], R. Barate[3b], D. Bloch[9], P. Bonamy[7], P. Borgeaud[7], M. Burchell[4], H. Burmeister[3], J.M. Brunet[6], F. Calvino[2a], M. Cattaneo[4], J.M. Crespo[2], B. d'Almagne[5], M. David[7], L. DiCiaccio[3c], J. Dixon[4], P. Druet[5], A. Duane[4], J.P. Engel[9], A. Ferrer[3d], T.A. Filippas[1], E. Fokitis[1], R.W. Forty[4], P. Foucault[9], E.N. Gazis[1], J.P. Gerber[9], Y. Giomataris[3], T. Hofmokl[10], E.C. Katsoufis[1], M. Koratzinos[3,4,5], C. Krafft[5], B. Lefievre[6], Y. Lemoigne[7], A. Lopez[3,5*], W.K. Lui[8], C. Magneville[7], A. Maltezos[1], J.G. McEwen[8], Th. Papadopoulou[1], B. Pattison[3], D. Poutot[6], M. Primout[7], H. Rahmani[1], P. Roudeau[5], C. Seez[4], J. Six[5], R. Strub[9], D. Treille[3], P. Triscos[6], G. Tristram[6], G. Villet[7], A. Volte[6], M. Wayne[5], D.M. Websdale[4], G. Wormser[5] and Y. Zolnierowski[3]

(The NA14/2 Collaboration)

(Submitted to Zeitschrift für Physik C)

1) National Technical University, Athens, Greece.
2) Universidad Autónoma de Barcelona, Bellaterra, Spain.
3) CERN, Geneva, Switzerland.
4) Blackett Lab., Imperial College, London, UK.
5) LAL, IN2P3–CNRS and Univ. Paris-Sud, Orsay, France.
6) Collège de France, Paris, France.
7) DPhPE, CEN–Saclay, Gif-sur-Yvette, France.
8) Univ. of Southampton, Southampton, UK.
9) CRN, IN2P3–CNRS and Univ. L. Pasteur, Strasburg, France.
10) Univ. of Warsaw, Warsaw, Poland.
a) Univ. Politecnica de Catalunya, ETSEIB–DEN, Barcelona, Spain.
b) Univ. J. Fourier and ISN, Grenoble, France.
c) Univ. di Roma II, 'Tor Vergata', Rome, Italy.
d) Univ. de Valencia, IFIC, Valencia, Spain.
*) On leave from Fac. de Ciencias Fisicas, Univ. Complutense, Madrid, Spain.

ABSTRACT

Properties of D mesons produced in the photoproduction experiment NA14/2 at CERN are reported. The following ratios of branching fractions were measured:

$$\mathrm{Br}(D^0 \to K^+K^-)/\mathrm{Br}(D^0 \to K^-\pi^+) = 0.16 \pm 0.05$$
$$\mathrm{Br}(D^0 \to K^-\pi^+\pi^0)/\mathrm{Br}(D^0 \to K^-\pi^+) = 4.0 \pm 0.9 \pm 1.0$$
$$\mathrm{Br}(D^0 \to K^-\pi^+\pi^+\pi^-)/\mathrm{Br}(D^0 \to K^-\pi^+) = 1.9 \pm 0.25 \pm 0.20 \ .$$

The $D^0 \to K^-\pi^+\pi^+\pi^-$ decay was analysed and the contribution of resonant subprocesses found consistent with 1 ρ^0 and 0.23 $\bar{K}^{*0}$ per event. The angular distributions of $D^0 \to \bar{K}^{*0}\rho^0$ showed parity violation and destructive interference between S- and D-waves.

From a Dalitz-plot analysis of the decay $D^+ \to K^-\pi^+\pi^+$ the contribution from the quasi two-body decay $D^+ \to \bar{K}^{*0}\pi^+$ was measured to be $0.14 \pm 0.04 \pm 0.04$.

1. INTRODUCTION

Samples of charmed particles have been obtained in the photoproduction experiment NA14/2 at CERN, using a high-resolution vertex detector. In Sections 2 and 3 we present a brief description of the apparatus and the data-processing procedure. We have measured the branching ratios for some of the D^0 decay modes*) and these are given in Section 4. The study of the $D^0 \to K^-\pi^+\pi^+\pi^-$ decay mode is presented in Section 5 and the Dalitz-plot analysis of the $D^+ \to K^-\pi^+\pi^+$ in Section 6.

2. APPARATUS AND TRIGGER

The NA14 experiment [1] is characterized by a large angular acceptance for photons and charged particles. For the study of charmed particles it has been equipped with a high-resolution silicon vertex detector [2]. This consists of a segmented silicon target with analogue readout and a set of ten planes of 50 μm pitch microstrips with an active area of 5 $\times$ 5 cm^2 and digital readout. The decay and production vertices are reconstructed using the microstrips. A 15 μm (300 μm) precision is achieved in the transverse (longitudinal) direction with respect to the beam. Charged particles are deflected by two magnets and measured by 73 planes of multiwire proportional chambers (MWPCs), which provide a high track-reconstruction efficiency and a momentum resolution of $\Delta p/p^2 = 5 \times 10^{-4}$ (GeV/c)$^{-1}$. Kaons are identified between 6.3 GeV/c and 20.5 GeV/c by an air-filled gas Cherenkov counter. Three electromagnetic calorimeters are used to reconstruct photons and neutral pions. For both charged and neutral particles, the geometrical acceptance is $\pm$ 300 mrad in the laboratory reference frame. This ensures unbiased detection efficiency for the different D decays.

A total of 17 million events were obtained using a high-energy bremsstrahlung photon beam, between 50 and 200 GeV. The trigger required at least two charged particles, one above and one below the horizontal region, to emerge from the interaction of the photons in the target.

3. DATA PROCESSING

The data used for this D^0 and D^+ study were first processed through a filter. A fast algorithm reconstructed the charged particles using the MWPC information. These tracks were then matched with microstrip hits and the position of the primary vertex along the beam line was defined using information from the active target. The charmed-particle content of the data was enhanced by rejecting events for which the tracks were

*) Charge-conjugate states are implicitly included throughout this paper.

compatible with a single vertex. This filter retained 18% of the sample to be processed through the full reconstruction programs. Its efficiency for charmed-particle decays was measured to be between 45% and 60%, depending on the nature of the charmed particle and its decay channel.

The full pattern-recognition program matches the MWPC tracks with microstrip hits and performs global track fits, after which vertices are reconstructed.

For a given charmed-particle decay, the appropriate combination of tracks is chosen using the Cherenkov counter information. If an acceptable decay vertex is found, the trajectory of the charmed-particle candidate is reconstructed and used in a fit with the remaining tracks in the event to search for the production vertex. If the fit is not acceptable, the least well associated track in this fit is rejected and the process is iterated. This procedure allows us to extract charmed-particle signals by requiring a cut on $N_\sigma = \Delta x/\sigma_x$, the separation (scaled by its error) between the production and the decay vertices, measured along the beam direction. The active target information is used to reject secondary interactions that mimic charmed-particle decay.

In order to obtain lifetimes [1], branching ratios [3], and cross-sections [4] from the data, it was necessary to correct for the geometrical acceptance of the apparatus, the reconstruction efficiencies, and the kinematic cuts used in the data selection. These corrections have been determined from a detailed Monte Carlo simulation of the experiment. The Monte Carlo events were analysed with the same set of programs as used for the data.

4. D^0 BRANCHING RATIOS

We present D^0 branching ratios relative to the decay channel $D^0 \to K^-\pi^+$.

The total $D^0 \to K^-\pi^+$ sample shown in Fig. 1 is the result of two different analyses. The $D^0 \to K^-\pi^+$ issuing from the cascade decay $D^{*+} \to D^0\pi^+ \to K^-\pi^+\pi^+$ was obtained using a cut on $N_\sigma > 0.5$. The direct $D^0 \to K^-\pi^+$ events were obtained after requiring $N_\sigma > 2$. A fit to the data yields a signal of 580 ± 41 events within the mass interval $1.83 < M_{K\pi} < 1.88$ GeV/c^2 and a signal-to-background ratio equal to 1.06.

The selection procedure applied to the $D^0 \to K^-\pi^+$ sample is adapted to each channel studied in order to minimize the systematic errors.

A search for the Cabibbo-suppressed decay mode $D^0 \to K^-K^+$ (Fig. 2) yielded a signal of 34 ± 10 events with a signal-to-background ratio equal to 1.0 within the mass interval $1.83 < M_{K^-K^+} < 1.875$ GeV/c^2. This was obtained using a cut $N_\sigma > 5$. Unambiguous kaon identification in the Cherenkov counter cannot be imposed for the analysis of this channel without a severe acceptance loss, so the kaon identification

criteria are relaxed to include particles with momentum greater than the kaon threshold (20.5 GeV/c). As a result, enhancements are seen on both the high and low mass sides of the D^0 peak, corresponding respectively to the decays $D^0 \to K^-\pi^+$ and $D^0 \to K^-\rho^+ \to K^-\pi^+\pi^0$ in which the pion has been assigned the kaon mass. The same selection cuts have been applied for the $D^0 \to K^-K^+$ and $D^0 \to K^-\pi^+$ channels in order to have the same geometrical and kinematical acceptances. In this case, this cancels most of the systematic errors. The ratio of branching fractions measured is

$$\frac{\mathrm{Br}(D^0 \to K^+K^-)}{\mathrm{Br}(D^0 \to K^-\pi^+)} = 0.16 \pm 0.05 \ .$$

For the $D^0 \to K^-\pi^+\pi^0$ decay, the π^0 was reconstructed using the γ's identified in the forward electromagnetic calorimeter [1]. This calorimeter registers about 90% of useful γ's for this decay mode. The typical energy resolution obtained from this lead-glass array is $0.15/\sqrt{E}$. The $\gamma\gamma$ effective mass spectrum has an r.m.s. of 15 MeV/c^2 at the π^0 mass. To improve the $K^-\pi^+\pi^0$ mass resolution we performed a kinematic fit of the π^0 by varying the impact positions and the energies of the γ candidates. To select the $D^0 \to K^-\pi^+\pi^0$ signal we required $N_\sigma > 8$. The sample obtained is shown in Fig. 3. The signal represents 69 $\pm$ 16 events within the mass interval $1.8 < M_{K^-\pi^+\pi^0} < 1.9$ GeV/c^2 with a signal-to-background ratio equal to 0.7. The intrinsic γ detection efficiency ϵ_γ (i.e. for photons within the geometrical acceptance of the calorimeter) was evaluated by two independent methods. We first assume, from isospin considerations, that the number of π^0 produced in hadronic events is one half the number of charged pions. By changing a $\pi^\pm$ into a π^0 we can then simulate the two-γ decay and thus calculate the value ϵ_γ for our detector. The second method is based on an analysis of clusters in the calorimeter. We computed $\epsilon_\gamma = 0.52$ and $\epsilon_\gamma = 0.49$ respectively using the two methods. We adopted the value $\epsilon_\gamma = 0.50 \pm 0.03$ and found

$$\frac{\mathrm{Br}(D^0 \to K^-\pi^+\pi^0)}{\mathrm{Br}(D^0 \to K^-\pi^+)} = 4.0 \pm 0.9 \pm 1.0 \ .$$

The systematic error on this ratio is mainly due to the uncertainty of the photon energy resolution in the Monte Carlo program.

To select the $D^0 \to K^-\pi^+\pi^+\pi^-$ decay, we required $N_\sigma > 3$ and obtained a signal of 337 $\pm$ 30 events within the mass interval $1.82 < M_{K^-\pi^+\pi^+\pi^-} < 1.89$ GeV/c^2 with a signal-to-background ratio equal to 0.8.

We obtained the following value:

$$\frac{\mathrm{Br}(D^0 \to K^-\pi^+\pi^+\pi^-)}{\mathrm{Br}(D^0 \to K^-\pi^+)} = 1.90 \pm 0.25 \pm 0.30 \ .$$

The systematic error is dominated by the uncertainty in charged-track detection efficiency, for which a detailed analysis has been performed.

5. STUDY OF THE DECAY $D^0 \to K^-\pi^+\pi^+\pi^-$

The $K^-\pi^+\pi^+\pi^-$ final state allows an interesting investigation of the D decays into pseudoscalar + axial vector [$K^- a_1^+$, $\pi^+ K_1^-$ (1270)] and into vector + vector ($\bar{K}^{*0}\rho^0$) mesons. In order to reduce the background, we have applied a vertex separation cut $N_\sigma > 10$. Events from the $D^{*+} \to D^0\pi^+$ cascade were also used with a relaxed vertex separation cut $3 < N_\sigma < 10$. The resulting sample contained a signal $N_{D^0} = 213 \pm 21$ events with a signal-to-background ratio of 1.7 (Fig. 4a). In Figs. 5–9, the experimental points are shown after subtraction of the non-D^0 background taken from the wing regions: $1.74 < M_{K\pi\pi\pi} < 1.815$ and $1.89 < M_{K\pi\pi\pi} < 1.965$ GeV/c^2. The signal was defined in the interval $1.83 < M_{K\pi\pi\pi} < 1.875$ GeV/c^2.

5.1 Search for $D^0 \to \bar{K}^{*0}\rho^0$ decays

The amounts of $\rho^0(N_\rho)$ and $\bar{K}^{*0}(N_{K^*})$ contained in the $D^0 \to K^-\pi^+\pi^+\pi^-$ sample were obtained from the $\pi^+\pi^-$ and $K^-\pi^+$ mass distributions shown in Fig. 5. There are two $\pi^+\pi^-$ and two $K^-\pi^+$ mass combinations for each event. A 50% combinatorial background is thus added to the non-resonant background. In our fits we parametrized the latter two backgrounds using a polynomial multiplied by a threshold factor $(M - M_t)^{1/2}$, where M_t is the threshold mass. A Breit–Wigner term was added coherently for the resonance contribution. The fits shown in Fig. 5 were obtained using a quadratic polynomial, and the Breit–Wigner mass and width fixed at world average values. The shapes of the background distributions resulting from the fits are also shown. They are similar to those of the $\pi^+\pi^-$ and $K^-\pi^+$ wrong combinatorial combinations obtained for $D^0 \to \bar{K}^{*0}\rho^0$ decays generated by Monte Carlo simulation. Systematic errors due to the parametrization of the non-resonant background were estimated to be about 10 and 6% respectively for the fraction of ρ^0 and $\bar{K}^{*0}$.

For the $\pi^+\pi^-$ mass distribution (Fig. 5a) we get $N_\rho/N_{D^0} = 0.98 \pm 0.12 \pm 0.10$, indicating that the $D^0 \to K^-\pi^+\pi^+\pi^-$ is consistent with all final states containing a ρ^0. For the $K^-\pi^+$ mass distribution (Fig. 5b) we get $N_{K^*}/N_{D^0} = 0.23 \pm 0.06 \pm 0.06$.

Assuming one ρ^0 per event we find

$$\frac{\mathrm{Br}(D^0 \to [K^-\pi^+]_{\mathrm{nr}}\rho^0)}{\mathrm{Br}(D^0 \to K^-\pi^+\pi^+\pi^-)} = 0.77 \pm 0.06 \pm 0.06 \ ,$$

$$\frac{\mathrm{Br}(D^0 \to \bar{K}^{*0}\rho^0 \to K^-\pi^+\pi^+\pi^-)}{\mathrm{Br}(D^0 \to K^-\pi^+\pi^+\pi^-)} = 0.23 \pm 0.06 \pm 0.06 \ .$$

These ratios agree with the result of the Fermilab experiment E–691 [5]. Taking into account the isospin factor 2/3 for the $\bar{K}^{*0}$ decay and using [6] $\mathrm{Br}(D^0 \to K^-\pi^+\pi^+\pi^-) = 0.091 \pm 0.008 \pm 0.008$, we obtain:

$$\mathrm{Br}(D^0 \to \bar{K}^{*0}\rho^0) = 0.031 \pm 0.008 \pm 0.008 \ .$$

5.2 Search for $D^0 \to K^- a_1^+$ decays

Since 77% of the events have a ρ^0 and no $\bar{K}^{*0}$ in the final state, we searched for evidence of the following decay chain:

$$D^0 \to K^- a_1^+ \to K^- \pi^+ \rho^0 \to K^- \pi^+ \pi^+ \pi^- \ .$$

We selected 85 decays with no $K^-\pi^+$ mass combination within $\pm$ 50 MeV of the $\bar{K}^{*0}$ mass and with at least one $\pi^+\pi^-$ combination within $\pm$ 150 MeV of the ρ^0 mass. These cuts also select the three-body decay $D^0 \to K^-\pi^+\rho^0$.

Owing to the large width of the a_1^+ meson the three-pion effective mass distribution cannot be used to separate the amount of $K^- a_1^+$ and $K^-\pi^+\rho^0$ events. Nevertheless evidence of the sequential decay through a_1^+ can be investigated using helicity arguments [7]. Since the D^0 is spinless, the a_1^+ must be in a zero helicity state. Hence the final state must have a $\cos^2\ \theta^*$ distribution, where θ^* is the angle between the direction of the a_1^+ in the D^0 rest frame and the direction of the π^- in the ρ^0 rest frame. There are two $\pi^+\pi^-$ combinations for the three-pion system, one coming from the ρ^0 decay; the other combination, called wrong, is identical to the $\pi^+\pi^+$ system. Thus we have subtracted the $\pi^+\pi^+$ system from the distribution of the two $\pi^+\pi^-$ combinations. Monte Carlo calculations have shown that the θ^* distributions of the 'wrong' $\pi^+\pi^-$ combination and the $\pi^+\pi^+$ combination are affected by the selection cuts (no $K\pi$ in the K^* band and at least one $\pi^+\pi^-$ in the ρ band), but that, after subtraction, the generated θ^* distribution of the 'right' $\pi^+\pi^-$ combination (from the ρ^0) could be recovered. The $\cos\ \theta^*$ angular distribution is shown in Fig. 6 together with the $D^0 \to K^- a_1^+$ Monte Carlo events (full-line histogram).

The corresponding angular distribution for the three-body decay has been generated by Monte Carlo simulation with an S-wave between the K^- and the π^+. The dotted-line histogram represents this distribution using the same selection cuts and analysis procedure as used for the data.

Owing to our limited statistics, both hypotheses investigated in this analysis are compatible with the data.

5.3 Search for $D^0 \to \pi^+ K_1^-$ (1270) decays

Although the $K^-\pi^+\pi^+\pi^-$ final state is consistent with one ρ^0 per event, within the errors there is room for $D^0 \to \pi^+ K_1^-$ (1270). Several decay chains of this axial vector lead to the $K^-\pi^+\pi^+\pi^-$ final state. Using the compiled branching fractions [8], we computed $Br(K_1^-(1270) \to K^-\pi^+\pi^-) = 0.36 \pm 0.04$, of which 60% have no ρ^0 in the final state.

The K_1^-, having a smaller width than the a_1^+, was sought in the $K^-\pi^+\pi^-$ mass distribution (Fig. 7). Only the combination with the lower $\pi^+\pi^-$ mass was used since Monte Carlo calculations have shown that 65% of the K_1^- signal is expected for this combination.

No statistically significant enhancement is observed in the $K_1(1270)$ region. A fit to a polynomial background and a Breit–Wigner term yields 18 ± 21 events. Correcting for the $K^-\pi^+\pi^-$ combinations with the higher $\pi^+\pi^-$ mass we get the branching fraction:

$$\mathrm{Br}(D^0 \to \pi^+ K_1^-(1270)) = 0.03 \pm 0.04,$$

where the error is statistical only.

5.4 Angular distribution of $D^0 \to \bar{K}^{*0}\rho^0$ decays

A selected subsample of $D^0 \to \bar{K}^{*0}\rho^0$ was obtained by requiring the $K^-\pi^+$ mass and the remaining $\pi^+\pi^-$ mass to be within $\pm$ 1Γ of the $\bar{K}^{*0}$ and ρ^0 mass respectively. This cut improved the signal-to-background ratio to 5.1 (Fig. 4b). The signal is 85 ± 10 events. About 63% of this subsample are two-body $\bar{K}^{*0}\rho^0$ events (Fig. 8a). No K^* is observed in the $K^-\pi^+$ mass distribution for the events with the remaining $\pi^+\pi^-$ mass below 620 MeV/c^2 (Fig. 8b). Furthermore, the combinatorial background due to the two π^+ per event is much reduced. There are about 1.05 combinations per event within the cuts.

The decay angular distribution can be described using three angles θ_1, θ_2, and χ defined in the Appendix. The 'folded' distribution of the azimuthal angle χ (Fig. 9a) shows that the decay planes of ρ^0 and $\bar{K}^{*0}$ are preferentially parallel rather than orthogonal. Monte Carlo calculations have shown that this effect is not due to our experimental acceptance, which was found to be uniform for the angle χ. The distributions of the polar angles θ are expected to be identical for the two vector mesons and were added together (Fig. 9b).

The differential distributions for these two angles can then be parametrized according to the following expressions:

$$\frac{dn}{d\chi} \propto 1 + \beta \cos(2\chi)$$

$$\frac{dn}{d\cos\theta} \propto \delta + \gamma \cos^2\theta.$$

The parameters β and γ can be related to the amount of S-, P- and D-waves present in the decay amplitude as given in the Appendix. The parameter δ has been fixed at 1 except in the case of a pure D-wave, where $\delta = 0$. This pure D-wave is excluded by our data and thus we fit the formula with $\delta = 1$. In Table 1 we compare our measurements with the expectations from a single angular momentum state.

As the measured β value is close to the pure S-wave expectation, there is no need for a large P-wave component. The measured γ value can only be reproduced if we assume that S- and D-waves are contributing and if they interfere destructively.

Defining the relative fractions f_P and f_D of the contributions of P- and D-waves with respect to the S-wave and denoting by ϕ_D the relative phase between the S- and the D-wave (see Appendix) we have fitted simultaneously the χ and θ distributions. Both parameters β and γ are functions of the three variables, f_P, f_D, and ϕ_D. Thus, these fits cannot give a single determination of the relative contribution of each wave. Nevertheless, boundaries of f_P and f_D were obtained and are displayed in Fig. 10.

Acceptable solutions involve large destructive interference between S- and D-waves ($\cos\phi_D \leq -0.8$) and a contribution from parity-violating amplitudes larger than 80%.

In the unfolded χ distribution (χ now defined between 0 and π) an asymmetry of about $\pi/2$ involves the contribution of the parity-conserving P-wave interfering with the S-wave such that $\sin\phi_P \neq 0$. This behaviour is clearly observed (Fig. 11) and is well reproduced by the expected γ distribution given in the Appendix. Our results are consistent with $\sin\phi_p > 0.9$.

6. STUDY OF THE DECAY $D^+ \to K^-\pi^+\pi^+$

The three-body decay $D^+ \to K^-\pi^+\pi^+$ can proceed via a two-body vector + pseudoscalar decay, $\bar{K}^{*0}\pi^+$. Our aim is to study this process and to extract the fraction of two-body decays.

The D^+ signal shown in Fig. 12 was obtained by selecting events which have a reconstructed primary vertex and a three-prong secondary vertex downstream of the primary vertex with a separation cut $N_\sigma > 4$. The D^+ signal used in the analysis was selected in the mass interval $1.83 \leq M_{K\pi\pi} \leq 1.89$ GeV/c^2; the background under the signal was obtained by a linear interpolation from the side regions into the peak ($1.77 < M_{K\pi\pi} < 1.82$ and $1.90 < M_{K\pi\pi} < 1.95$ GeV/c^2). The result yielded a signal of 394 ± 33 events, with a signal to background ratio of 1.1

The fraction of the quasi two-body final state ($\bar{K}^{*0}\pi^+$) was determined by fitting the Dalitz plot (with two entries per event), using a maximum likelihood method. In order to evaluate the geometrical acceptance, we generated Monte Carlo events which were then reconstructed and analysed with the same set of programs as used for the data. The detection efficiency was found to be uniform over the Dalitz plot. Figure 13 shows the $K^-\pi^+$ (2 combinations per event) and $\pi^+\pi^+$ mass-squared projections after background subtraction. The background used was taken from both sides of the peak signal (Fig. 12).

The $M^2_{K\pi}$ distribution (Fig. 13a) shows three features. A $\bar{K}^{*0}(890)$ signal, a broad bump between 1.0 and 1.9 $(GeV/c^2)^2$, and a depletion between 2.0 and 2.4 $(GeV/c^2)^2$. This distinctive behaviour has been seen in two other experiments [9, 10]. In the $M^2_{\pi\pi}$ distribution (Fig. 13b) we expect no resonant structure.

The likelihood function used a coherent sum of phase space and Breit–Wigner functions:

$$\mathcal{L}_N = \prod_{j=1}^{N} \mid \alpha_{ps} + e^{i\phi_R}\alpha_R[B_{K\pi_1}W(\theta_{K\pi_1}) + B_{K\pi_2}W(\theta_{K\pi_2})] \mid^2$$

normalized over the Dalitz plot where

- B is the relativistic Breit–Wigner function, with energy-dependent width [11],
- $W(\theta) = \cos\theta$ is the angular distribution of the $\bar{K}^{*0}$ decay,
- α_{ps} and α_R are the coefficients of the three-body phase space and $\bar{K}^{*0}$ resonance, respectively,
- ϕ_R is the relative phase between the three-body phase space and the Breit–Wigner amplitudes.

The product extends over the total number of events (N) in the Dalitz plot.

We minimized, with respect to α_{ps}, α_R and ϕ_R, the logarithm of the likelihood function

$$-\ln\ \mathcal{L} = -\ln\ \mathcal{L}_{N_T} + r\ \ln\ \mathcal{L}_{N_B}\ ,$$

where N_T is the number of events in the D^+ peak (signal + background) N_B the number of events on either side of the peak signal, and r the statistical weight of the events used from the side regions. A χ^2 probability is calculated on the projections to evaluate the goodness of the fits.

The fraction of resonance production and phase space can be defined as:

$$R = \int_D \alpha_R^2 \mid B_{K\pi_1}W(\theta_{K\pi_1}) + B_{K\pi_2}W(\theta_{K\pi_2}) \mid^2 dM^2_{K\pi_1} dM^2_{K\pi_2}$$

$$ps = \int_D \alpha_{ps}^2 dM^2_{K\pi_1} dM^2_{K\pi_2}$$

normalized by the integral over the Dalitz plot of the squared sum of the amplitudes. The definition above implies that if there is interference between the different amplitudes, then the sum of the resonant and non-resonant components could be different from one.

The corresponding results are shown by the dotted lines in Fig. 13 and listed in Table 2. It is obvious from the curves that this simple model does not provide a good description of the special features of the data.

In order to improve the description we tried adding coherently in the likelihood function the well-known $K^*(1430)$ resonance or a non-resonant D-wave in the $\pi\pi$

amplitude. We were still unable to improve the fit to the structure at the end of the $K\pi$ phase space. Following the procedure adopted in Ref. 10 we add a Bose symmetric term, $\alpha\ e^{i\phi}\ |\ M^2_{K\pi_1} - M^2_{K\pi_2}\ |$. The result of this fit is shown as full lines in Fig. 13 and given in Table 2. Good agreement is found for the two projections.

The result obtained for this last fit, which yields the best χ^2, gives the ratio of branching fractions:

$$\frac{Br(D^+ \to \bar{K}^{*0}\pi^+ \to K^-\pi^+\pi^+)}{Br(D^+ \to K^-\pi^+\pi^+)} = 0.14 \pm 0.04 \pm 0.04\ .$$

The statistical error is derived from the error matrix of the fitted parameters. The systematic error is obtained by varying the cuts of the D^+ event selection and the statistical weight r of the background in the fits.

7. CONCLUSION

In the previous sections we studied D decays and obtained the following ratios of branching fractions:

$$Br(D^0 \to K^+K^-)/Br(D^0 \to K^-\pi^+) = 0.16 \pm 0.05$$
$$Br(D^0 \to K^-\pi^+\pi^0)/Br(D^0 \to K^-\pi^+) = 4.0 \pm 0.9 \pm 1.0$$
$$Br(D^0 \to K^-\pi^+\pi^+\pi^-)/Br(D^0 \to K^-\pi^+) = 1.9 \pm 0.25 \pm 0.20\ .$$

For the $D^0 \to \bar{K}^{*0}\rho^0$ decays, the $\bar{K}^{*0}$ and the ρ^0 decay planes were found to be preferentially parallel, reflecting the contribution of the parity-violating S-wave. The combined analysis of the polar and azimuthal angular distributions gives boundaries of the relative contributions of the P- and D-waves with respect to the S-wave, and shows destructive interference between the S- and D-waves.

The $D^+ \to K^-\pi^+\pi^+$ decay channel shows unusual features in the $(K\pi)$ mass distribution which are not well described by a simple model of $K^*\pi$ interfering with a non-resonant $K\pi\pi$ system.

APPENDIX

The weak decay $D(p) \to V_1(k,\varepsilon_1)\ V_2(q,\varepsilon_2)$ can be described by the most general invariant matrix element as a sum of three terms:

$$M = aA_S + b\,e^{i\phi_D} A_D + ic\,e^{i\phi_P} B_P \ ,$$

where A_S and A_D are the parity-violating amplitudes of the S- and D-waves; B_P is the parity-conserving amplitude of the P-wave [12]. The scalars a, b, and c are real. The angles ϕ_D and ϕ_P are the phase shifts of the D- and P-wave amplitudes relative to the S-wave.

We define the polar angles θ_1 and θ_2 of the decay products in the $V_1(\bar{K}^{*0})$ and in the $V_2(\rho^0)$ rest frames respectively by

$$\cos\ \theta_1 = \frac{\vec{s}\cdot\vec{k}}{|\,\vec{s}\,|\cdot|\,\vec{k}\,|} \quad and \quad cos\ \theta_2 = \frac{\vec{t}\cdot\vec{q}}{|\,\vec{t}\,|\cdot|\,\vec{q}\,|} \ ,$$

where $\vec{s}$ and $\vec{t}$ are the momenta of the K^- and π^- in the $V_1(\bar{K}^{*0})$ and the $V_2(\rho^0)$ rest frames respectively; $\vec{k}$ is the momentum of the $V_1(\bar{K}^{*0})$ in the D^0 rest frame and $\vec{q} = -\vec{k}$ (Fig. 14).

The relative azimuthal angle $\chi = \varphi_1 - \varphi_2$ between the $V_1(\bar{K}^{*0})$ and $V_2(\rho^0)$ decay planes in the D^0 rest frame is defined by

$$\cos\ \chi = \frac{(\vec{s}\wedge\vec{k})(\vec{t}\wedge\vec{k})}{|\,\vec{s}\wedge\vec{k}\,||\,\vec{t}\wedge\vec{k}\,|} \ .$$

Denoting the masses and polarization vectors of V_1 and V_2 by m_1, m_2 and ε_1, ε_2, respectively, the amplitudes A and B are given by

$$\begin{aligned}
A_S &= \varepsilon_1\cdot\varepsilon_2 = \alpha\ \cos\ \theta_1\ \cos\ \theta_2 - \ \sin\ \theta_1\ \sin\ \theta_2\ \cos\ \chi \\
A_D &= \frac{1}{m_1 m_2}(p\cdot\varepsilon_1)(p\cdot\varepsilon_2) = (\alpha^2-1)\ \cos\ \theta_1\ \cos\ \theta_2 \\
B_P &= \frac{1}{m_1 m_2}\varepsilon^{\alpha\beta\gamma\delta}\varepsilon_{1\alpha}\varepsilon_{2\beta}k_\gamma p_\delta = \sqrt{\alpha^2-1}\ \sin\ \theta_1\ \sin\ \theta_2\ \sin\ \chi \ ,
\end{aligned}$$

where

$$\alpha = \frac{m_{D^0}^2 - m_1^2 - m_2^2}{2m_1 m_2}\ (\simeq 1.51 \text{ for } \bar{K}^{*0}\rho^0) \ .$$

Integrating $d^3n/(d\chi\ \mathrm{dcos}\ \theta_1\ \mathrm{dcos}\ \theta_2) \propto |\ M\ |^2$ over θ_1 and θ_2 gives the angular distribution of χ:

$$\begin{aligned}
\frac{9}{4}\frac{dn}{d\chi} =& a^2(\alpha^2+2) + b^2(\alpha^2-1)^2 + 2c^2(\alpha^2-1) \\
&+ 2ab\alpha(\alpha^2-1)\ \cos\ \phi_D \\
&+ 2[a^2 - c^2(\alpha^2-1)]\ \cos\ (2\chi) \\
&+ 4ac\sqrt{\alpha^2-1}\ \sin\ \phi_P\ \sin\ (2\chi) \ .
\end{aligned}$$

If this distribution, where χ is defined between 0 and π, is 'folded' around $\pi/2$ ($\chi = \cos^{-1}|\cos\chi|$) the last term cancels. We then obtain a simple form:

$$\frac{dn}{d\chi} \propto 1 + \beta\ \cos(2\chi)\ .$$

For example, for a pure S-wave ($b = c = 0$), $\beta = 2/(\alpha^2+2) \simeq 0.46$.

The polar angle distributions are identical for V_1 and V_2 and can be obtained from integration over θ_1 and χ:

$$\frac{3}{4\pi}\frac{dn}{d\cos\ \theta} = [a^2 + c^2(\alpha^2-1)] + (\alpha^2-1)[a^2 - c^2 + b^2(\alpha^2-1) + 2ab\alpha\ \cos\ \phi_D]\ \cos^2\theta\ .$$

Except for a pure D-wave, this expression reduces to

$$\frac{dn}{d\cos\ \theta} \propto 1 + \gamma\ \cos^2\theta\ .$$

For a pure S-wave, we have $\gamma = \alpha^2 - 1 \simeq 1.29$.

Finally, summing over all polarization variables yields

$$\frac{9}{8\pi}n = a^2(\alpha^2+2) + b^2(\alpha^2-1)^2 + 2c^2(\alpha^2-1) + 2ab\alpha(\alpha^2-1)\ \cos\ \phi_D\ ,$$

where the first three terms give the contributions of S-, D-, and P-waves respectively. The last term represents interference between D- and S-waves.

We define the relative fractions f_P and f_D of the contributions of P- and D-waves with respect to the S-wave by

$$f_P = \frac{2c^2(\alpha^2-1)}{a^2(\alpha^2+2)} \quad \text{and} \quad f_D = \frac{b^2(\alpha^2-1)^2}{a^2(\alpha^2+2)}\ .$$

REFERENCES

[1] P. Astbury et al., Phys. Lett. **B152** (1985) 419.
M.P. Alvarez et al. (NA14/2 Collaboration), Lifetime measurements of D^+, D^0, D_s^+ and Λ_c^+ charmed particles, preprint CERN–EP/90–26, to be published in Z. Phys. C.

[2] R. Barate et al., Nucl. Instrum. Methods, **A235** (1985) 235.
G. Barber et al., Nucl. Instrum. Methods, **A253** (1987) 530.

[3] M.P. Alvarez et al. (NA 14/2 Collaboration), Measurement of $D_S^{\pm}$ and Cabibbo-suppressed D^+ decays, preprint CERN–EP/90–65, to be published in Phys. Lett.

[4] M.P. Alvarez et al. (NA14/2 Collaboration), Study of charm photoproduction mechanisms (in preparation).

[5] J.C. Anjos et al. (Fermilab photoproduction experiment E-691), A study of the decay $D^0 \rightarrow K^-\pi^+\pi + -\pi^+$ and $D^+ \rightarrow k^-\pi^+\pi^+\pi^+\pi^-$, paper No. 402 contributed to the 24th Int. Conf. on High Energy Physics, Munich, 1988.

[6] J. Adler et al., Phys. Rev. Lett. **60** (1988) 89.

[7] P. Chong-Ho Kim, Thesis, University of Toronto, 1987 (unpublished).

[8] G.P. Yost et al., Particle Data Group, Phys. Lett. **B204** (1988) 1.

[9] R.H. Schindler et al., Phys. Rev. **D24** (1981) 78.

[10] J. Adler et al., Phys. Lett. **B196** (1987) 107.

[11] J.D. Jackson, Nuovo Cimento **34** (1964) 1644.

[12] G. Valencia, Phys. Rev. **D39** (1989) 3339.

Figure captions

Fig. 1 The $K^-\pi^+$ mass distribution of the $D^0 \to K^-\pi^+$ sample.

Fig. 2 The K^-K^+ mass distribution.

Fig. 3 The $K^-\pi^+\pi^0$ mass distribution of the $D^0 \to K^-\pi^+\pi^0$ sample.

Fig. 4 a) The $K^-\pi^+\pi^+\pi^-$ mass distribution after analysis cuts.
b) The $K^-\pi^+\pi^+\pi^-$ mass distribution of $D^0 \to \bar{K}^{*0}\rho^0$ candidates.

Fig. 5 a) The $\pi^+\pi^-$ distribution.
b) The $K^-\pi^+$ mass distribution.
The solid lines show the result of the fit and the dashed lines the non-resonant and combinatorial contributions (two combinations per event).

Fig. 6 Distribution of θ^*, the angle between the π^- in the ρ^0 rest frame and the three-pion system in the D^0 rest frame. The histograms are Monte Carlo predictions for $D^0 \to K^- a_1^+$ (full line) and $D^0 \to K^-\pi^+\rho^0$ (dashed line).

Fig. 7 The $K^-(\pi^+\pi^-)_{low}$ mass distribution. The curves are the results of the fit described in the text.

Fig. 8 The $K^-\pi^+$ mass distribution: a) for events with the remaining $\pi^+\pi^-$ mass within ± 150 MeV of the ρ^0 mass; b) for events with the $\pi^+\pi^-$ mass less than 620 MeV/c^2.

Fig. 9 a) Folded distribution of the angle χ between the $\bar{K}^{*0}$ and the ρ^0 decay planes. b) Sum of the distributions of the polar angles θ_1 and θ_2.
The curves are the result of the fits described in the text.

Fig. 10 Boundaries of the relative fractions f_P and f_D of the contributions of the P- and D-waves with respect to the S-wave.

Fig. 11 Unfolded distribution of the angle χ between the $\bar{K}^{*0}$ and the ρ^0 decay planes. The curve represents a fit to the expected angular distribution $1 + \beta \cos(2\xi) + \varepsilon \sin(2\xi)$.

Fig. 12 The $K^-\pi^+\pi^+$ mass distribution showing the D^+ signal.

Fig. 13 The $K^-\pi^+$ mass squared distribution (a) and the $\pi^+\pi^+$ mass squared distributions (b) of $D^+ \to K^-\pi^+\pi^+$ events. The curves are the result of the fits described in the text.

Fig. 14 Definition of the $D \to V_1(k, \varepsilon_1)\ V_2(q, \varepsilon_2)$ decay angles.

Table 1

Parameters of the decay angular distributions

	Data[a)]	S-wave	P-wave	D-wave
β	0.44 ± 0.18	0.46	-1	0
γ	-0.52 ± 0.32	1.29	-1	1
δ	1 (imposed)	1	1	0

a) The errors are statistical only.

Table 2

Results of the fits to the $D^+ \to K^-\pi^+\pi^+$ Dalitz plot

Likelihood function	Resonant fraction	Non-resonant fraction
$\mid \alpha_{ps} + e^{i\phi_R}\alpha_R[B_{K\pi_1}W(\theta_{K\pi_1}) + B_{K\pi_2}W(\theta_{K\pi_2})] \mid^2$	$0.10 \pm 0.04 \pm 0.03$	$0.75 \pm 0.08 \pm 0.04$
$\mid \alpha_{ps} + e^{i\phi}\alpha \mid M^2_{K\pi_1} - M^2_{K\pi_2} \mid +$ $e^{i\phi_R}\alpha_R[B_{K\pi_1}W(\theta_{K\pi_1}) + B_{K\pi_2}W(\theta_{K\pi_2})] \mid^2$	$0.14 \pm 0.04 \pm 0.04$	$0.76 \pm 0.05 \pm 0.05$

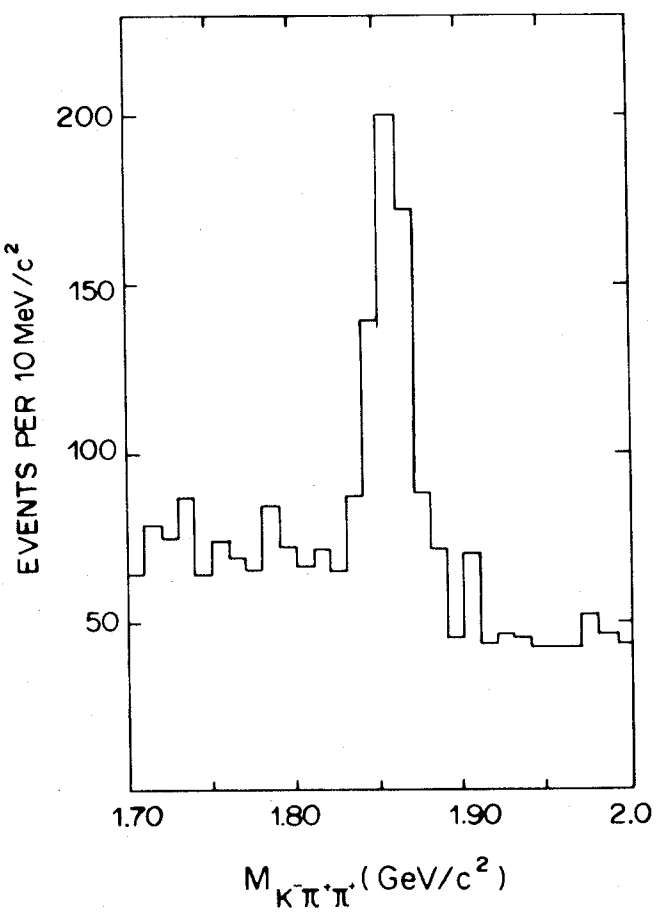
EVENTS PER 10 MeV/c²
200
150
100
50
1.70
1.80
1.90
2.0
M K⁻π⁺π⁺ (GeV/c²)

Fig. 1

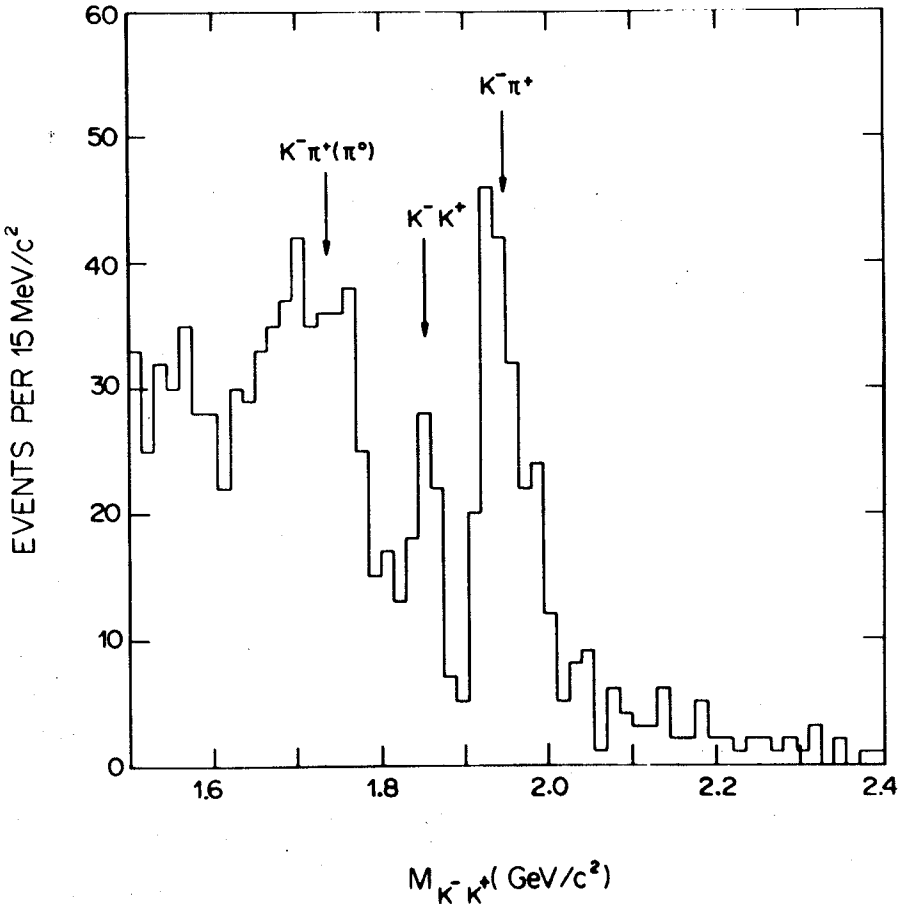
EVENTS PER 15 MeV/c²
60
50
40
30
20
10
0
K⁻π⁺(π°)
K⁻K⁺
K⁻π⁺
1.6
1.8
2.0
2.2
2.4
M K⁻K⁺(GeV/c²)

Fig. 2

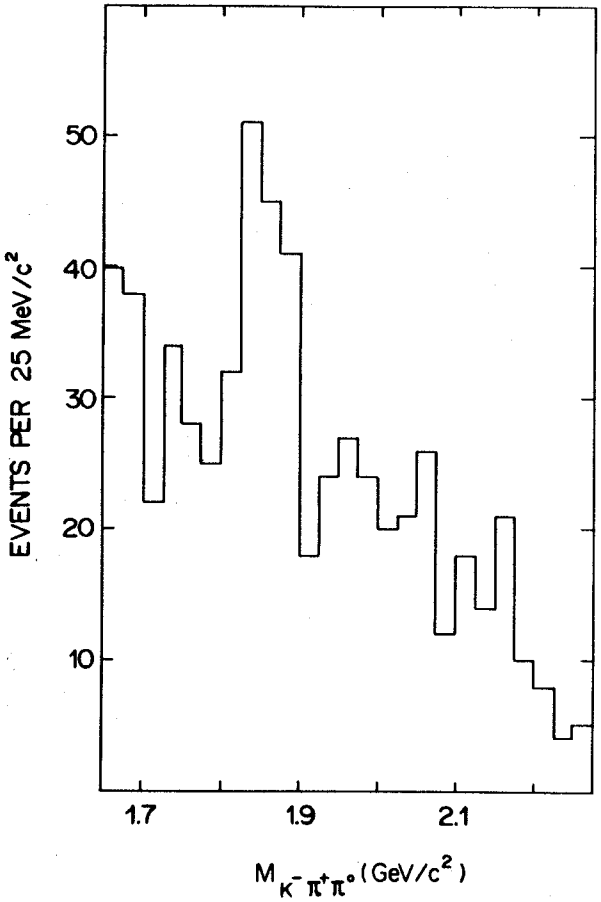
EVENTS PER 25 MeV/c²
50
40
30
20
10
1.7
1.9
2.1
M K⁻π⁺π°(GeV/c²)

Fig. 3

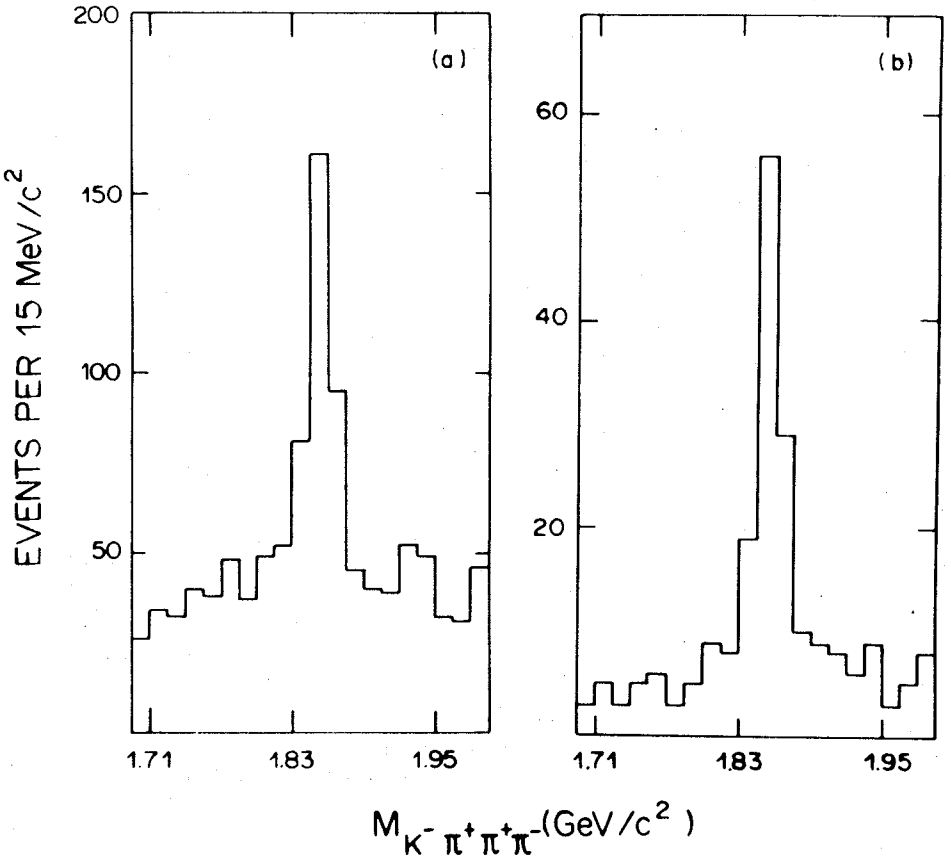
EVENTS PER 15 MeV/c²
200
150
100
50
(a)
(b)
60
40
20
1.71
1.83
1.95
1.71
1.83
1.95
M K⁻π⁺π⁺π⁻(GeV/c²)

Fig. 4

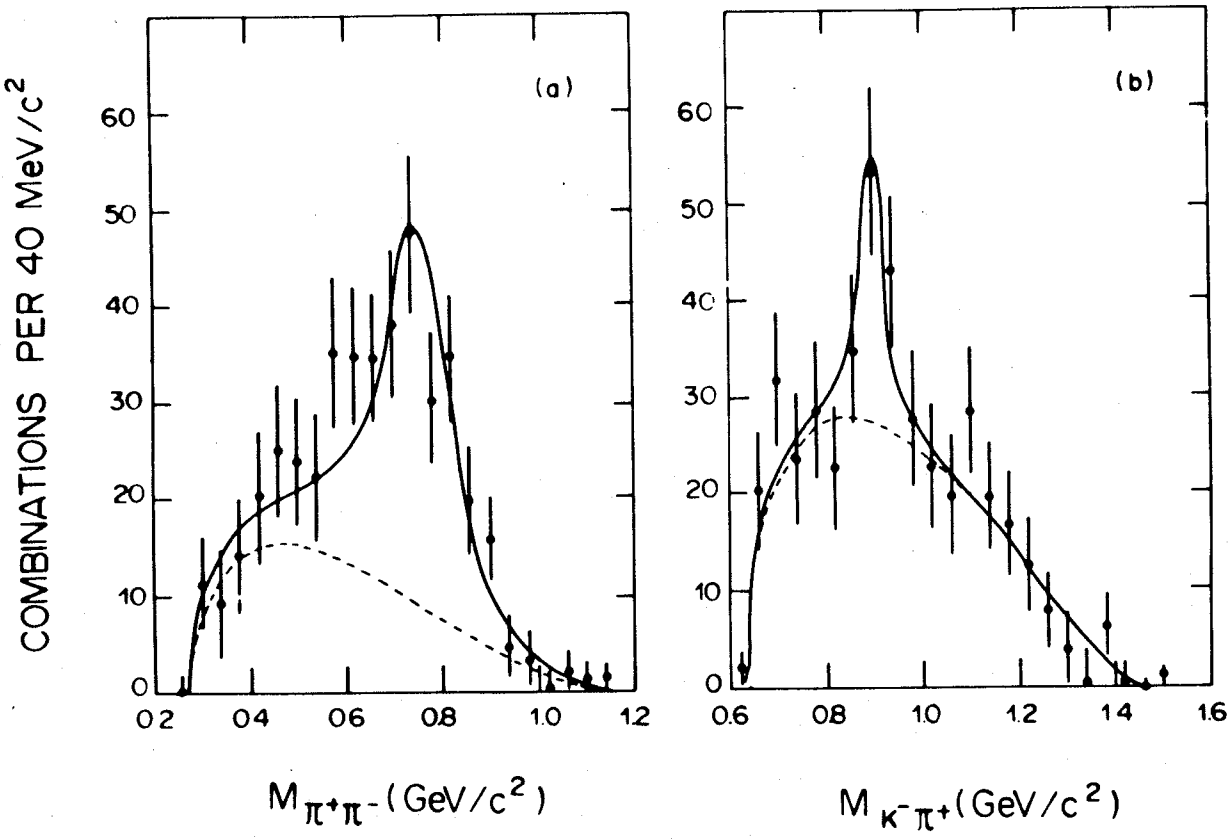
COMBINATIONS PER 40 MeV/c²
(a)
(b)
0
10
20
30
40
50
60
0.2
0.4
0.6
0.8
1.0
1.2
1.4
1.6
M π⁺π⁻ (GeV/c²)
M K⁻π⁺ (GeV/c²)

Fig. 5

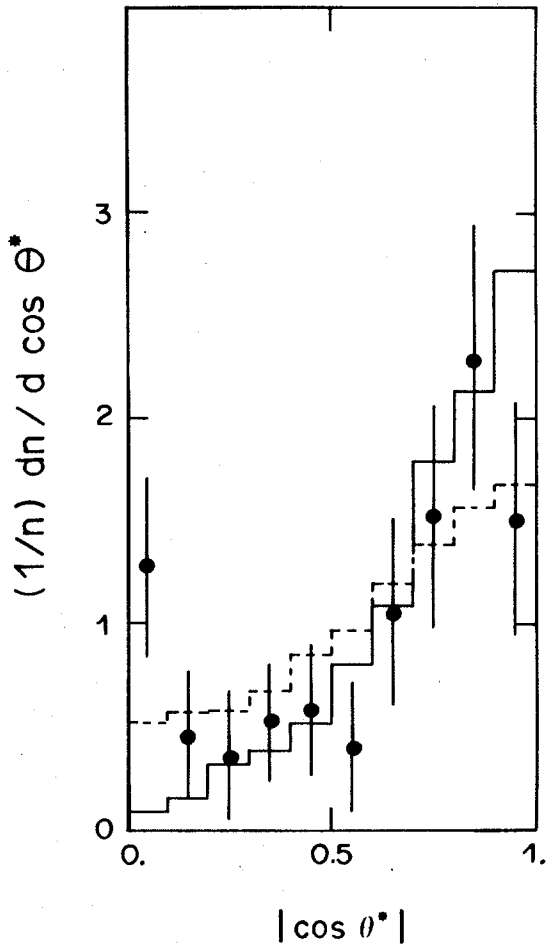
(1/n) dn / d cos Θ*
0
1
2
3
0.
0.5
1.
| cos θ* |

Fig. 6

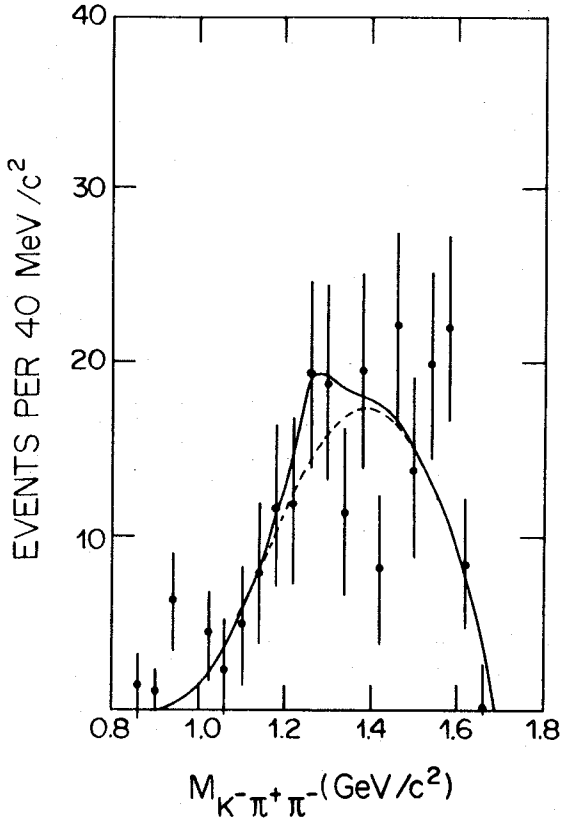
EVENTS PER 40 MeV/c²
40
30
20
10
0.8
1.0
1.2
1.4
1.6
1.8
M K⁻π⁺π⁻ (GeV/c²)

Fig. 7

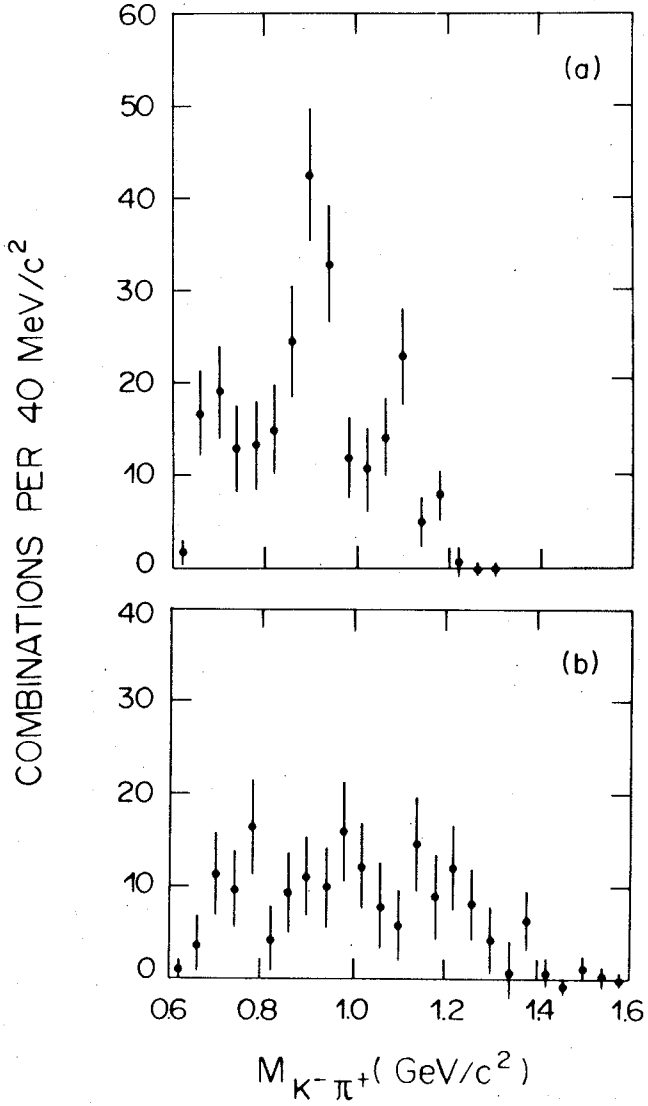
COMBINATIONS PER 40 MeV/c²
(a)
(b)
60
50
40
30
20
10
0
0.6
0.8
1.0
1.2
1.4
1.6
M K⁻π⁺ (GeV/c²)

Fig. 8

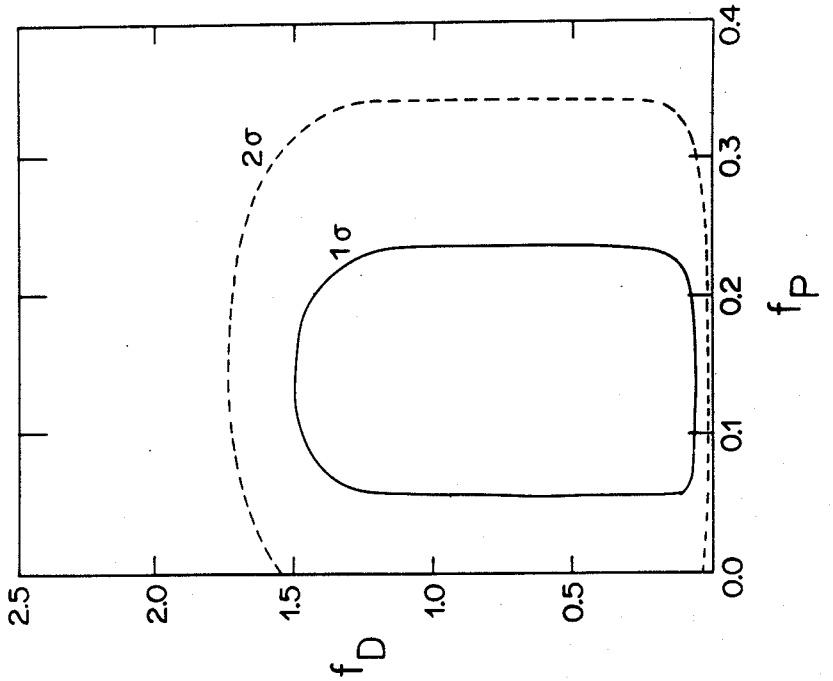
2σ
1σ
f_D
f_P
2.5
2.0
1.5
1.0
0.5
0.0
0.1
0.2
0.3
0.4

Fig. 10

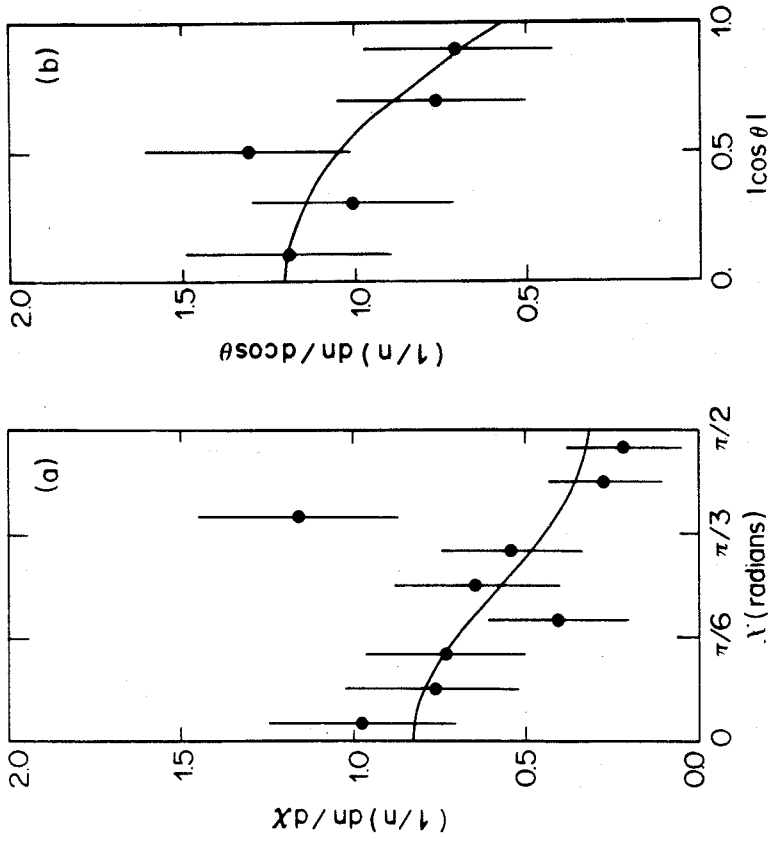
(a)
(b)
$(1/n)\,dn/d\chi$
$(1/n)\,dn/d\cos\theta$
χ (radians)
$|\cos\theta|$
0
π/6
π/3
π/2
0.5
1.0
1.5
2.0

Fig. 9

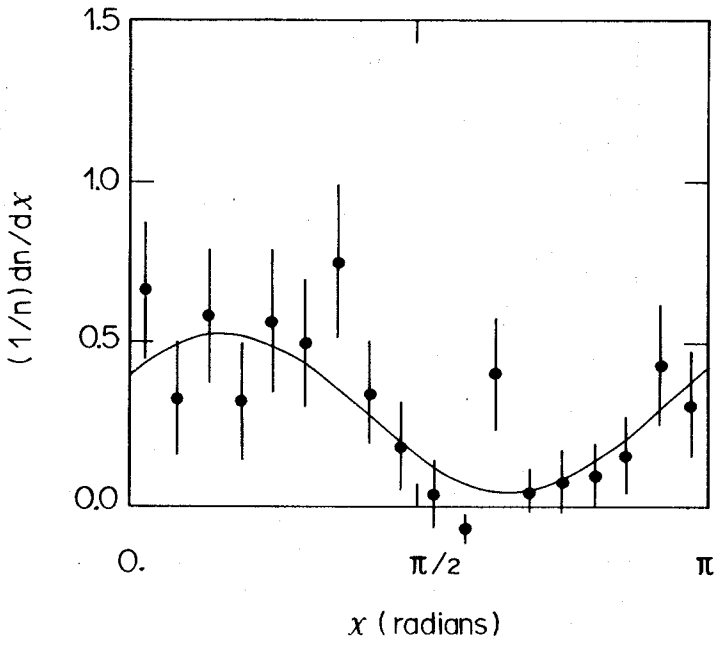
1.5
1.0
0.5
0.0
(1/n) dn/dx
0.
π/2
π
x (radians)

Fig. 11

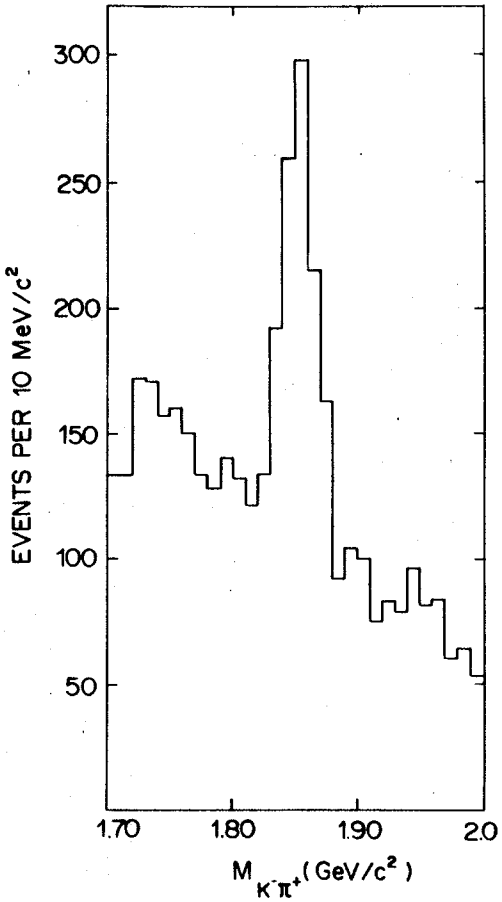
300
250
200
150
100
50
EVENTS PER 10 MeV/c²
1.70
1.80
1.90
2.0
M K⁻π⁺ (GeV/c²)

Fig. 12

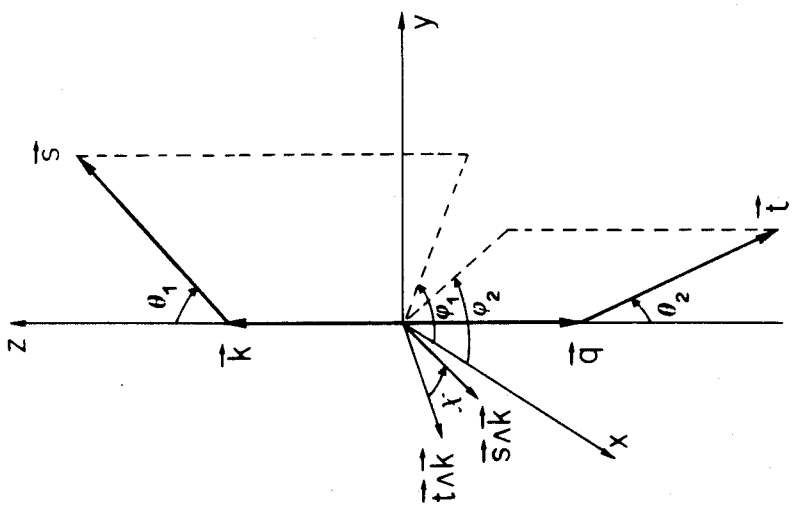

Fig. 14

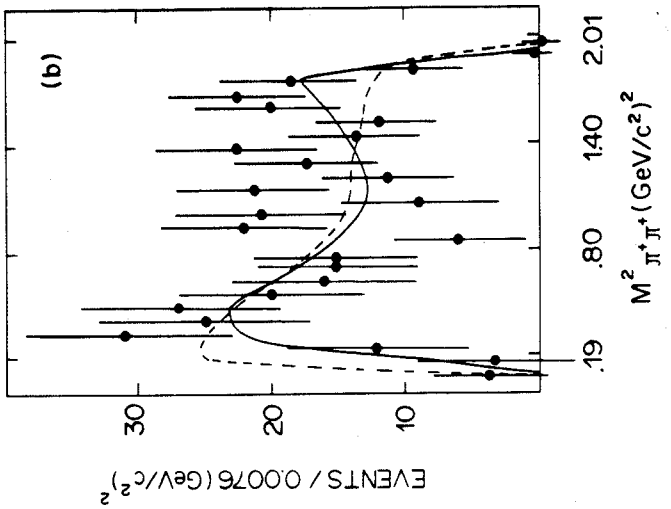

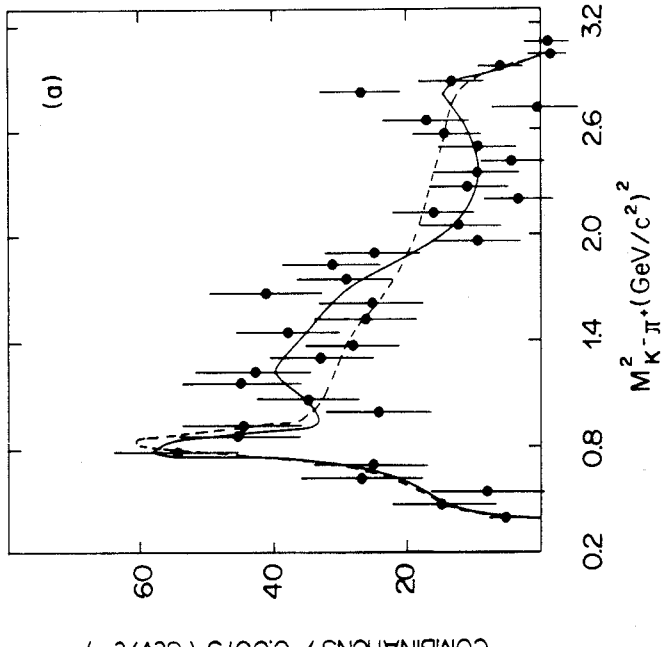

Fig. 13

Imprimé au CERN. Prix : 0.80 Fr.